Experimental demonstration of a millimeter-wave metallic ENZ lens based on the energy squeezing principle

Torres, Victor; Orazbayev, Bakhtiyar; Pacheco-Pena, Victor; Teniente, Jorge; Beruete, Miguel; Navarro-Cia, Miguel; Ayza, Mario Sorolla; Engheta, Nader

DOI:
10.1109/TAP.2014.2368112

Citation for published version (Harvard):
Torres, V, Orazbayev, B, Pacheco-Pena, V, Teniente, J, Beruete, M, Navarro-Cia, M, Ayza, MS & Engheta, N 2015, 'Experimental demonstration of a millimeter-wave metallic ENZ lens based on the energy squeezing principle', *IEEE Transactions on Antennas and Propagation*, vol. 63, no. 1, 6949057, pp. 231-239. https://doi.org/10.1109/TAP.2014.2368112

Experimental Demonstration of a Millimeter-Wave Metallic ENZ Lens based on the Energy Squeezing Principle

Víctor Torres, Bakhtiyar Orazbayev, Víctor Pacheco-Peña, Jorge Teniente, Miguel Beruete, Miguel Navarro-Cía, *Member, IEEE,* Mario Sorolla Ayza, *Senior Member, IEEE,* and Nader Engheta, *Fellow, IEEE*

***Abstract*—The performance of an epsilon-near zero (ENZ) plano-concave lens is experimentally demonstrated and verified at the D-band of the millimeter-waves. The lens is comprised of an array of narrow metallic waveguides near cut-off frequency, which effectively behaves as an epsilon-near-zero medium at 144 GHz. A good matching with free space is achieved by exploiting the phenomenon of energy squeezing and a clear focus with a transmission enhancement of 15.9 dB is measured. The lens shows good radiation properties with a directivity of 17.6 dBi and low cross-polar components of -34 dB. All results are supported by numerical simulations.**

***Index Terms*—Epsilon-near-zero, energy squeezing, metallic lenses, metamaterials, millimeter wave devices.**

I. Introduction

THE advent of metamaterials has opened new horizons in the control of electromagnetic waves owing to the possibility of engineering materials with almost any arbitrary value of constitutive parameters [1]. Recently, special attention has been paid to artificial materials with permittivity close to zero, the so-called epsilon-near-zero (ENZ) metamaterials [2]. Some natural materials show this feature at visible and infrared when working near their plasma frequencies [3]. However, as we are limited by the dispersive behavior of the medium, engineered materials are needed to tune the response in those regimes [4,5], and specially are essential for lower frequencies such as microwaves or millimeter waves where materials with vanishing permittivity are not naturally and easily available. In such ENZ structures, the phase velocity becomes near-infinite resulting in a quasistatic field distribution. This brings unconventional properties such as energy squeezing or electric field enhancement [2,6,7], among others. Exploiting these properties, ENZ materials are used in a wide range of applications such as radiation patterning [8,9], cloaking [10,11], subwavelength imaging [12], boosting of optical nonlinearities [13] or optical nanocircuits [14,15], to name a few.

ENZ materials are also suitable for developing lenses due to their ability of tailoring the wave fronts to desired shapes by simply controlling the lens profile [8]. In 1946, Kock proposed a plano-concave metallic lens made of conductive plates, taking advantage of the high phase velocity of a wave passing between the plates [16]. Subsequently, further realizations of metallic lenses working effectively with a near zero index of refraction have been proposed [17-24]. They are advanced designs that address the problem of impedance matching suffered by Kock lenses. In [17, 18], stacked subwavelength hole arrays displaying extraordinary transmission [25] were used to focus an incoming plane wave. In [19,20], the plasma-like behavior of the TE_1 mode of parallel plate waveguides was exploited to synthesize artificial dielectric lenses with a dispersive refractive index. In close relation with the work presented here, plano-concave and plano-plano ENZ metallic lenses made of narrow waveguides were proposed, designed and theoretically analyzed in [21, 22]. Further examples of graded-index lenses, based on apertures of non-uniform widths working in the visible, can be found in [23, 24].

In this work, we experimentally investigate and verify the performance of a plano-concave ENZ lens made of a metallic

This work was supported in part by the Spanish Government under contract Consolider Engineering Metamaterials CSD2008-00066 and contract TEC2011-28664-C02-01. VT is sponsored by the Universidad Pública de Navarra. BO is sponsored by Spanish Ministerio de Economía y Competitividad under grant no. FPI BES-2012-054909. VP-P is sponsored by Spanish Ministerio de Educación, Cultura y Deporte under grant no. FPU AP-2012-3796 and appreciates the support provided by the Navarra Government (Spain) under resolution 10/2011 of 7 April (BON no 79) 'Becas Navarra Talento Internacional'. MB is sponsored by the Spanish Government via RYC-2011-08221. MN-C is supported by the Imperial College Junior Research Fellowship.

V. Torres, B. Orazbayev, V. Pacheco-Peña, J. Teniente and M.Beruete are with the Antenna Group - TERALAB (MmW - THz – IR & Plasmonics Laboratory), Universidad Pública de Navarra, Pamplona 31006, Spain (e-mail: victor.torres@unavarra.es, b.orazbayev@unavarra.es victor.pacheco@unavarra.es, jorge.teniente@unavarra.es, miguel.beruete@unavarra.es).

M. Navarro-Cía is with the Optical and Semiconductor Devices Group, Department of Electrical and Electronic Engineering; Centre for Plasmonics and Metamaterials; and Centre for Terahertz Science and Engineering, Imperial College London, London SW7 2AZ, UK (e-mail: m.navarro@imperial.ac.uk).

M. Sorolla Ayza deceased, was with the TERALAB (MmW - THz – IR & Plasmonics Laboratory), Universidad Pública de Navarra, Pamplona 31006, Spain

N. Engheta is with the Department of Electrical and Systems Engineering, University of Pennsylvania, Philadelphia 19104, USA. (e-mail: engheta@ee.upenn.edu).

waveguide array working near the waveguide cut-off frequency, demonstrating experimentally the theory presented in [21, 22]. Two studies are presented here: the first is a characterization of the focal plane and the transmission properties; and second, a lens antenna arrangement is analyzed and the radiation characteristics are extracted. To the best of our knowledge, this is the first realization of an arrangement of near cut-off metallic waveguides used as an ENZ structure that tailors an incoming plane wave in a spherical focus, or vice versa, at a frequency of 144 GHz.

II. Design And Fabrication

The fabricated lens is shown in Fig. 1(a). It consists of a plano-concave aluminum structure of dimensions L_x = 76.2 mm, L_y = 86.2 mm, L_z = 40 mm and d = 55.5 mm where an array of 33 × 114 narrow apertures has been manufactured along the z-axis. Each aperture is a hollow metallic waveguide of cross-sectional dimensions h_x = 1.1±0.025 mm, h_y = 0.05±0.02 mm. These dimensions are chosen in order to work at a frequency around 140 GHz: since the electric field of the incoming wave is polarized along the y-axis, parallel to h_y, and $h_x > h_y$, the fundamental mode is the TE_{10}, whose cut-off frequency is $f_c^{TE10} = c/2h_x$ = 136.36 GHz, where c is the velocity of light in free space [26]. Slightly above this frequency, each waveguide behaves as an ENZ medium where the propagation constant is very small and thus the effective permittivity is very close to zero [2,6,7,21,22]. Moreover, in order to avoid the mismatch of the lens with free space, h_y is designed to be electrically very small ($\approx\lambda_0/42$) and hence the wave is able to tunnel through the structure coupling most of the energy at the output, a phenomenon that is known as energy squeezing (i.e., supercoupling) [6, 7]. The in-plane periodicity of the array is d_x ~ 1.4 mm and d_y ~ 0.5 mm. The lens profile is semi-spherical with a diameter d. Hence, the shortest waveguide that corresponds to the minimum thickness of the lens is 12.25 mm long. Due to fabrication limitations, the array of apertures does not cover the whole diameter of the sphere along the x-axis, see bottom-right inset in Fig. 1(a).

The fabrication process, done by the technological center Tekniker, was as follows: the array of waveguides comprises 114 aluminum sheets of thickness $t = d_y$ = 481.5±3.5 μm. Each sheet had initial dimensions of $L_x \times L_y$ where 33 slots of 1.1 mm × 0.05 mm × 40 mm ($h_x \times h_y \times L_z$) with a periodicity of d_x were etched with a high speed micro milling machine Kondia HS1000 that uses a jagged tool mounted on a ceramic bearing rotating at 24000 rpm. In order to ensure a uniform and tolerable roughness, the manufacturing process was done under cooling conditions. The average roughness of the sheets after the milling step is only 0.32 μm. Figure 1(b) shows a picture taken with a confocal microscope of one of the slot waveguides, where the roughness of the metallic walls can be appreciated. Subsequently, the 114 sheets were stacked and two thick aluminum blocks were placed on the upper and lower part, to serve as bases. The whole structure was tightened with eight metallic crosspieces in order to ensure perfect electrical contact between adjacent plates. The alignment and dimensional characterization of the sheets was made by optical microscopy. After that, the semi-sphere was mechanized by means of die-sinking electrical discharge machining using a copper electrode that guarantees sphericity during the whole process. Finally, the apertures were cleaned with an ultrasonic washer.

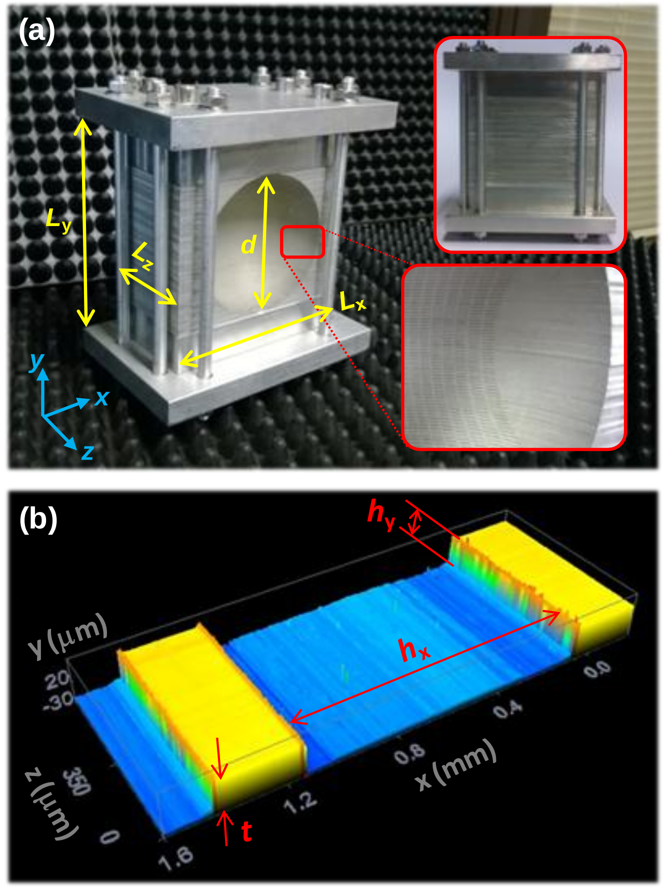

Fig. 1. (a) Photograph of the plano-concave ENZ metallic lens. (upper inset) View of the flat face of the lens. (lower inset) Detail of narrow waveguides in the concave profile. (b) Photograph taken with a confocal microscope of one of the slots etched in the aluminum sheets.

III. Results

A. Focal plane characterization

Experimental results were obtained in this subsection with two different setups and compared with simulations in Fig. 2-4. A sketch of the first setup is depicted in Fig. 2(b). The flat face of the lens was illuminated with a D-band corrugated horn antenna generating a y-polarized Gaussian beam. The feeder was placed 1.3 m away from the flat face of the lens. At this distance, the beam radius of the Gaussian beam radiated by the corrugated horn antenna is 138 mm for 140 GHz, ensuring quasi-uniform illumination of the flat face of the lens. A WR-6.5 rectangular waveguide with its standard flange was used as a receiver, which was fixed on a motorized 2-axis translation stage with a minimum step of 0.5 mm in both x and z or y axes. Raster scanning was done to find the focus at any desired frequency. Both transmitter and receiver were connected to an AB-Millimetre™ Quasioptical Vector Network Analyzer (VNA) which covers the spectrum 0.04 - 1

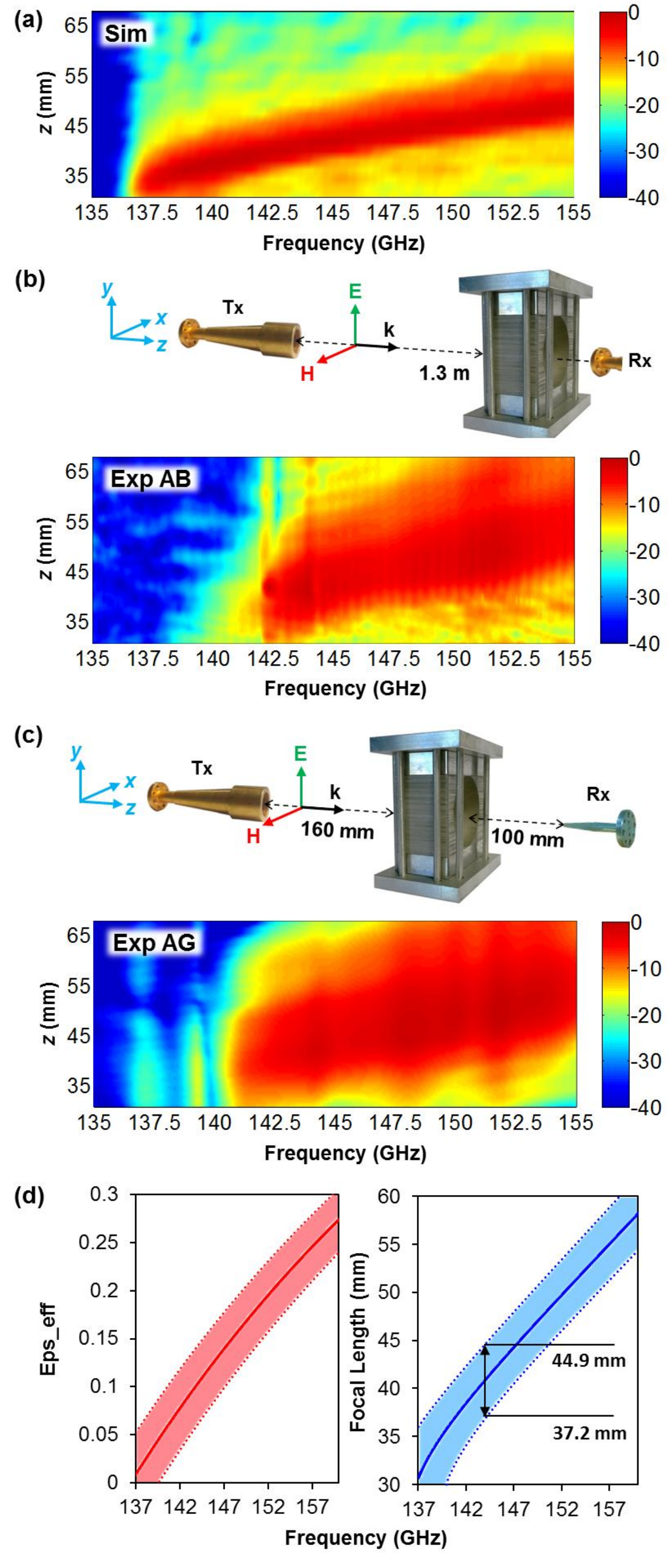

Fig. 2. (a) Simulated (Sim) normalized transmission enhancement spectra along the optical *z*-axis. (b) Sketch of the first experimental set-up and measured (*Exp AB*) normalized transmission enhancement spectra using the AB Millimetre VNA and the flange-ended WR-6.5 waveguide as a receiver (Rx). (c) Sketch of the second experimental set-up and measured (*Exp AG*) normalized transmission enhancement spectra using the Agilent VNA and the WR-8.0 near-field waveguide probe as a receiver (Rx). (d) Analytical calculation of the effective permittivity and the focal length for the nominal value of the hollow waveguide together with the maximum deviation induced by the fabrication tolerances (h_x = 1.1±0.025 mm).

THz. The transmission with the horn antenna and the flange-ended WR-6.5 waveguide placed face to face without the lens in between is used as reference, i.e., calibration. The whole setup was covered with radar absorbing material (RAM) to mimic anechoic chamber conditions. Experimental results obtained with this setup are named *Exp AB* from now on.

Given the large size of the flange surrounding the WR-6.5 waveguide, the detection carried out with the first setup is invasive. To mitigate the effect of the detector, a second experimental setup (Fig. 2(c)) was used with a near-field probe with sharpened edges. In this case the setup used OML millimeter-wave heads connected to an Agilent Technologies N5242A PNA-X network analyzer. The feeder is the same horn antenna as in the first setup but in this case it was placed 160 mm away from the flat face of the lens. At this distance, the width of the Gaussian beam is reduced up to 33 mm. Despite the flat face not uniformly illuminated, it was easier to cover the interaction between transmitter and receiver with a metallic plate and RAM, and similar performance was obtained with a Gaussian beam excitation [22]. Both transmitter and receiver OML millimeter-wave heads were connected to an Agilent N5242A PNA-X Network Analyzer. A waveguide probe in WR-8.0 was used as a receiver, which was fixed on a motorized 2-axis translation stage. Raster scanning was done in a rectangle of 320 mm × 320 mm with a step of 0.8 mm parallel to the *xy*-plane at 100 mm away from the exit face of the lens of the lens, 135 to 155 GHz frequency bandwidth was collected (201 points) and a narrow time gating was applied to isolate the remaining reflection of the setup. The receiver was covered with RAM to avoid undesired reflections. With these measured values of the transversal components of the electric field, and after proper mathematical backtransformation, the field in any transversal plane in the *z*-axis can be obtained [27]. The results measured with this setup are denoted as *Exp AG*.

Simulation results were performed with CST Microwave Studio™ using the transient solver. The whole 3D-lens was modeled according to fabrication dimensions, including the bases on the top and bottom but excluding the crosspieces. The lens was illuminated with a plane wave letting the solver run until the remaining energy inside the calculation domain was below -60 dB the peak value to ensure validity of the continuous-wave (frequency) results obtained via Fourier transformation. Given the two-fold symmetry, magnetic and electric mirror planes were used at *yz*- and *xz*-planes, respectively, in order to reduce computation volume and time. A general hexahedral mesh of resolution equal to $\lambda_0/10$ was used by default for the simulation box. However, the waveguides hollow dimension h_y was further refined up to a resolution of $\lambda_0/170$. The total number of mesh cells was ~36,700,000. The lens material was aluminum (Al) with conductivity σ_{Al} = 3.56 × 10^7 S/m, which appropriately models well-polished Al layers at millimeter waves [28].

In Fig. 2(a), the simulated transmission enhancement spectra along the optical *z*-axis are presented. For this result, the waveguide receiver was not modeled to reduce computation effort. From this color map one can immediately estimate the frequency of operation. In an ideal situation, the ENZ lens should start exactly above f_c^{TE10} = 136.36 GHz, showing a focus at the center of the semi-sphere (x = 0, y = 0, z = 22.5). However, it is known that the matching condition, and thus, the energy squeezing phenomenon, is slightly blue-shifted [10,21,22]. This can be seen in the figure; transmission rises at 136.60 GHz but the maximum happens at 140.73 GHz. This frequency shift implies that the effective permittivity deviates from zero, since $\varepsilon_{eff} = 1-(f_c^{TE10}/f)^2$ and therefore the ideal quasistatic behavior is partially lost. Hence, the phase front at the exit face does not follow exactly the spherical profile, and thus, aberrations are expected. Evidence of this fact is the increase of the focal length accompanied by the widening of the depth of focus as the frequency increases.

Regarding the experimental results obtained with the AB Millimetre VNA (*Exp AB*), we also observe an abrupt transmission level of 27 dB from the experimental lower cutoff frequency of the lens at ~138 GHz to the peak frequency found at ~144 GHz. The increment of the focal length with frequency is noted as well. However, ripples are observed in the color map, not observed in the simulation, which are caused by standing waves between the lens and the flanged-ended WR-6.5 waveguide, as the second setup reveals. In Fig. 2(c) the experimental results obtained with the Agilent VNA (*Exp AG*) are shown. Now the ripple is not present, confirming the previous argument based on standing waves. Moreover, transmission rises at 141.5 GHz and the maximum happens at 144.3 GHz in very good agreement with the previous experimental results. From now on f_0 = 144 GHz (λ_0 = 2.08 mm), will be considered the working frequency of the ENZ lens.

Experimental results show a blue-shift in frequency as well as an increase in the focal length, which can arguably be attributed to fabrication tolerances. To support this assumption, the dispersion of the effective permittivity and the focal length for the nominal value of the hollow waveguide together with the maximum deviation introduced by the fabrication tolerances (h_x = 1.1±0.025 mm) is shown in Fig. 2(d). According to this analytical calculation, the ENZ lens at f_0 exhibits an effective permittivity ε_{eff} = 0.103. The tolerances can induce a deviation of the focal length of approximately ±4 mm centered ~141 GHz. Namely, at f_0 the focus is expected to be located between 37.2 mm and 44.9 mm in agreement with the results of Fig. 2(b) and 2(c).

To characterize the image space of the lens for the working frequency f_0, two additional transmittance maps are obtained. The *yz*-maps at x = 0 mm are shown in Fig. 3(a, c, e, g). From the results measured with the first setup (*Exp AB*), Fig. 3(a), it is evident that the energy is mostly focused around the center of the *y*-axis, as expected for the symmetry conditions. However, the results are not perfectly symmetric, possibly caused by some misalignments in the setup. The maximum is located at z = 40.25 mm, in agreement with the results from Fig. 2(b). Moreover, a ripple is again observed along the *z*-axis.

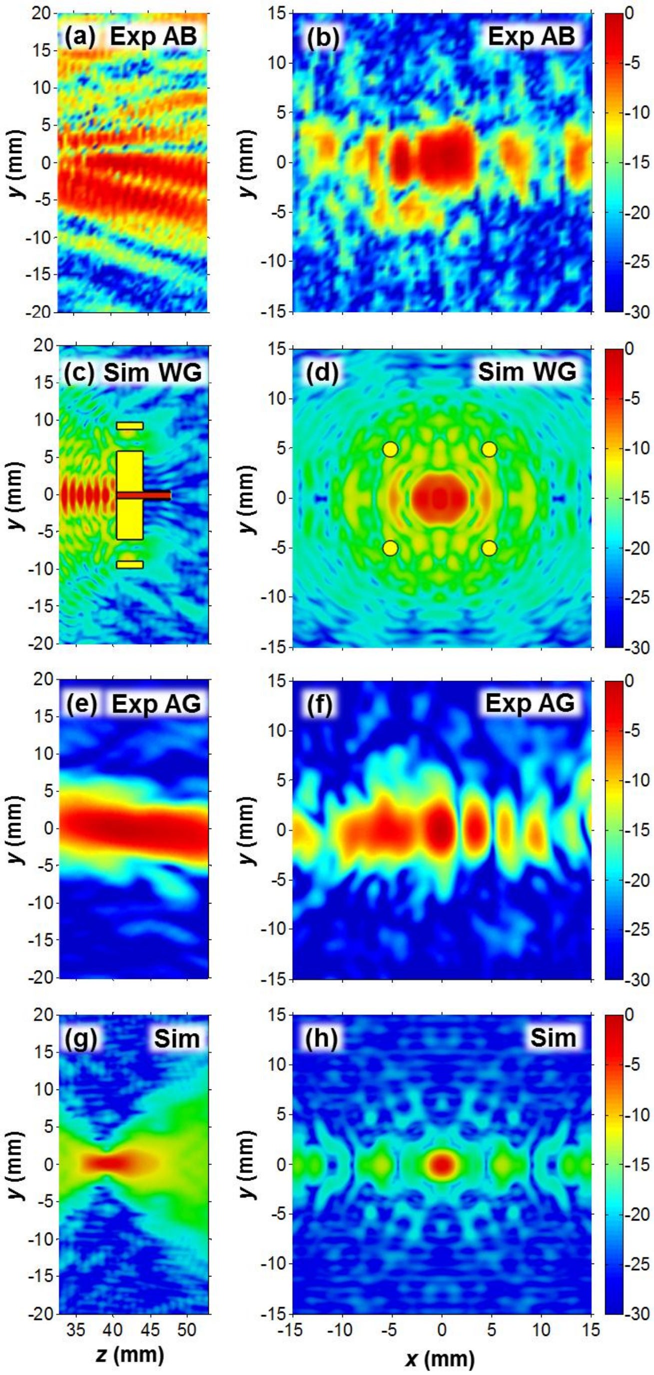

Fig. 3. Normalized transmission enhancement (a, e) measured and (c, g) simulated on the *yz*-plane; and (b, f) measured and (d, h) simulated on the *xy*-plane at the working frequency of 144 GHz (a-d, g,h) and 144.3 GHz (e, f). *Exp AB* and *Exp AG* refer to experimental results obtained with the AB Millimetre VNA and Agilent VNA setup, respectively. *Sim WG* and *Sim* correspond to simulations with and without the model of the detector, respectively. The yellow rectangles in panel (c) outline the standard flange of the WR-6.5.

The simulation result, Fig. 3(c), also displays the experimental main features. Notice that, unlike Fig. 2(a), the WR-6.5 waveguide along with its standard flange has been now modeled (Sim WG). Figure 3(c) shows unquestionably that Fabry-Perot resonances appear between the flange-ended WR-6.5 waveguide and the lens as a result of the large flange

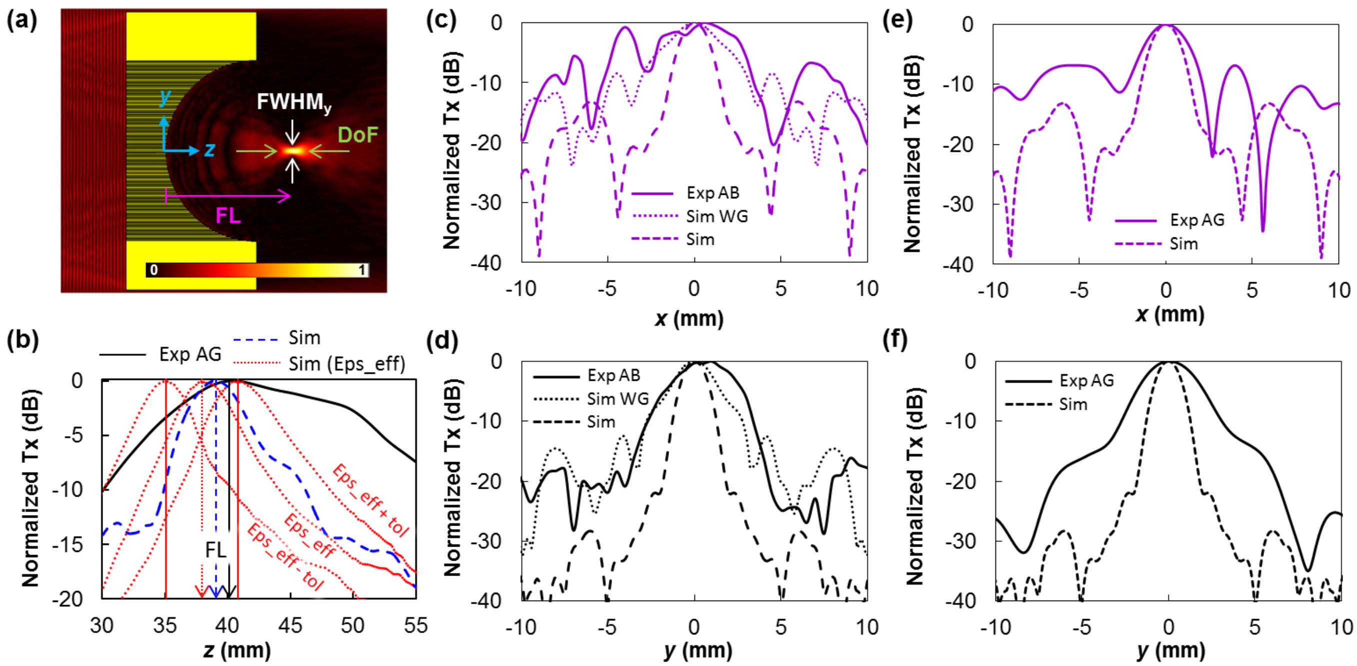

Fig. 4. (a) Numerically-computed magnitude of the electric field normalized to the maximum on the *yz*-plane at the working frequency f_0=144 GHz. (b) Normalized transmission along the z-axis for *x*=*y*=0 mm at f_0 where the focal length is marked with vertical arrows. Continuous line (Exp AG) represents measured values with Agilent VNA setup, dotted line (Sim) simulated values of the full lens and dashed line (Sim(Eps_eff)) simulated values of the lens formed by homogenous material. (c, e) Normalized transmission at f_0 along the *x*-axis and (d, f) along the *y*-axis at the FL. Exp AB and Exp AG represent experimental results obtained with the AB Millimetre and Agilent VNA setup, respectively. Sim WG and Sim represent simulation results with and without the modeling of the detector, respectively.

of the detector. This argument is corroborated further with the second setup, Fig. 2(e), where the amount of metal facing the lens is reduced to the frame of the waveguide probe. The second set of measurements has no sign of standing waves and shows a better focus performance in agreement with Fig 3(g), which shows the simulation result without modeling the detector. The symmetry along the *y*-axis is now well observed and the maximum is located at *z* = 40.40 mm, similarly to the first set of experiments.

Once the maximum of the focus along the *z*-axis was found, a *xy*-plane scanning was done at that particular *z* to find its position on this plane, see transmission results in Fig. 3(b, d, f, h). A very clear energy enhancement is observed in the experiments (Fig. 3(b) and 3(f)) around the center of the plane (*x*=*y*=0 mm) where the theoretical position of the focus is located. However, some differences as well as further points in common are observed in both results. On the one hand, the focus recorded with *Exp AB* has a larger extension than the focus obtained in *Exp AG*. This is an effect of the flange-ended WR-6.5 waveguide as can be deduced from the simulations. The ideal simulation (Sim) of Fig. 2(h) shows a more concentrated focus than the simulation including the waveguide (Sim WG). On the other hand, several secondary lobes are also noticed in all results along *x*- as well as *y*-axis, although the latter have lower values. The fact that the secondary lobes along the *x*-axis are higher than those along the *y*-axis is related with the effective aperture. As described in the fabrication section, the concave profile does not have waveguides all along the *x*-axis, causing the effective length to be 17% lower than the *y*-axis, and therefore, the energy focusing is worse along *x*. Finally, regarding the maximum transmission enhancement (maximum power received with respect to the case without the ENZ lens), we measure a maximum value in the focus equal to 15.9 dB in *Exp AB* in good agreement with the simulated value of 16.77 dB. It must be highlighted that in *Exp AG* the maximum obtained is only 5.61 dB since the non-uniform illumination produces a high penalty in the maximum transmission, as demonstrated in [22].

Let us now compare in depth the numerical and experimental results in terms of the focusing properties. In Fig. 4(a), the numerically-computed magnitude of the electric field on the *yz*-plane at the working frequency f_0 is shown. We observe how the impinging plane wave is tailored in a quasi-circular wave front resulting in a good focusing of the field. The focal length (FL), the depth of focus (DoF) along the optical axis (*z*-axis), and the full-width at half-maximum (FWHM) (see Fig. 4(a) for graphical representation of these lens properties) can be extracted from this two-dimensional color map and its *xz* counterpart. The transmission along the optical axis for $x = y = 0$ mm is depicted in Fig. 4(b). In the experiment (solid black curve) the FL = 40.40 mm, in good agreement with the simulation (dashed blue curve) where FL = 38.91 mm. Regarding the DoF, in the experiment we obtain a DoF = 14.8 mm = 7.11λ_0 while in the simulation is DoF = 3.94 mm = 1.9λ_0. It must be noted that a spatial averaging is introduced by the receiver and a wider focus than the simulation is expected, where an ideal point detector is assumed, and therefore this comparison must be done with precautions. Both results are compared with the simulation for a plano-concave lens with the same dimensions of the waveguide array and formed by an isotropic homogenous material with a permittivity equal to ε_{eff} = 0.103 (dotted red curve). A FL = 38.17 mm and DoF = 4.37 mm are calculated, similar to the ones obtained with the waveguide array. This underlines the effectiveness of modeling the lens as a medium with effective ENZ. Furthermore, similar simulations were performed for ε_{eff} = 0.061 (dotted red curve labelled as *Eps_eff - tol*) and ε_{eff} = 0.143 (dotted red curve labelled as *Eps_eff + tol*) which correspond with the limits of the effective permittivity delimited by the fabrication tolerances (h_x = 1.1±0.025 mm). It can be seen that the measured FL is within the limits predicted by the fabrication, and therefore, tolerances can explain the discrepancy between experiment and simulation. From these results the ENZ lens can be assumed to exhibit an effective epsilon of ε_{eff} = 0.138.

TABLE I
SUMMARY OF THE FOCUS PERFORMANCE

	FL[a]	DoF[b]	FWHM[c]		Max. Tx.[d]
			x-axis	*y-axis*	
Exp AB	40.25 mm	10.4 mm $5\lambda_0$	4.60 mm $2.21\lambda_0$	3.51 mm $1.69\lambda_0$	15.90 dB
Sim WG	38.91 mm	-	2.76 mm $1.33\lambda_0$	2.26 mm $1.08\lambda_0$	14.75 dB
Exp AG	40.40 mm	14.8 mm $7.11\lambda_0$	2.36 mm $1.13\lambda_0$	3.04 mm $1.46\lambda_0$	5.61 dB
Sim	38.91 mm	4.59 mm $2.21\lambda_0$	1.63 mm $0.78\lambda_0$	1.45 mm $0.69\lambda_0$	16.77 dB

[a]FL is the focal length
[b]DoF is the depth of focus
[c]FWHM is the full-width at half-maximum
[d]Max. Tx. is the maximum transmission enhancement

This study is completed by analyzing the focus in the *xy*-plane. The transmission along the *x*- and *y*-axis at the focal length is depicted in Fig. 4(c-f). Figure 4(c, d) compares *Exp AB* with two sets of simulation results: with and without modeling the detector. It is evident from these results that the WR-6.5 waveguide along with its flange introduce important differences. The simulation without the WR-6.5 waveguide shows a narrower focus in both axis and lower secondary lobes than *Exp AB*. However, when the flange-ended WR-6.5 waveguide is modeled, the numerical prediction agrees reasonable well with *Exp AB*. Meanwhile, *Exp AG* (Fig. 4(e, f)) is better reproduced by the simulation without the detector than *Exp AB* because of a minor influence of the probe. Now the focus is narrower and the secondary lobes lower. Nevertheless, the simulation does not match completely *Exp AG* yet, due to the spatial averaging introduced by the receiver and the different illumination conditions. In general, the overall performance (first null beam width (FNBW), secondary lobes and minimums) is in good agreement in both experiment and simulation results. A summary of all these results is shown in Table I. There is no result for DoF in Sim WG because that simulation was done only for the particular case of the detector placed at the FL.

B. ENZ lens antenna: radiation characteristics

Finally, the ability of the ENZ lens to improve the radiation properties of a poorly directive source is analyzed. Now, we use only the setup with the Agilent VNA. A waveguide probe WR-5.1 (as low directivity radiator) is situated at the experimental focus and used as a feeder while a waveguide probe WR-8.0 was used as a receiver. A raster scanning was done with the latter in a rectangle of 200 mm × 200 mm with a step of 0.8 mm parallel to the *xy*-plane at 100 mm away from the exit face of the lens. The measured fields in this *xy*-plane allow us to calculate via planar near-field to far-field transformation the fields in the far-field region and therefore the radiation pattern [27]. A sketch of this new setup is depicted in Fig. 5(a). Notice that the end of the WR-8.0 is now included in the simulation, but not the WR-5.1 probe, and a far-field monitor is used to obtain the radiation pattern.

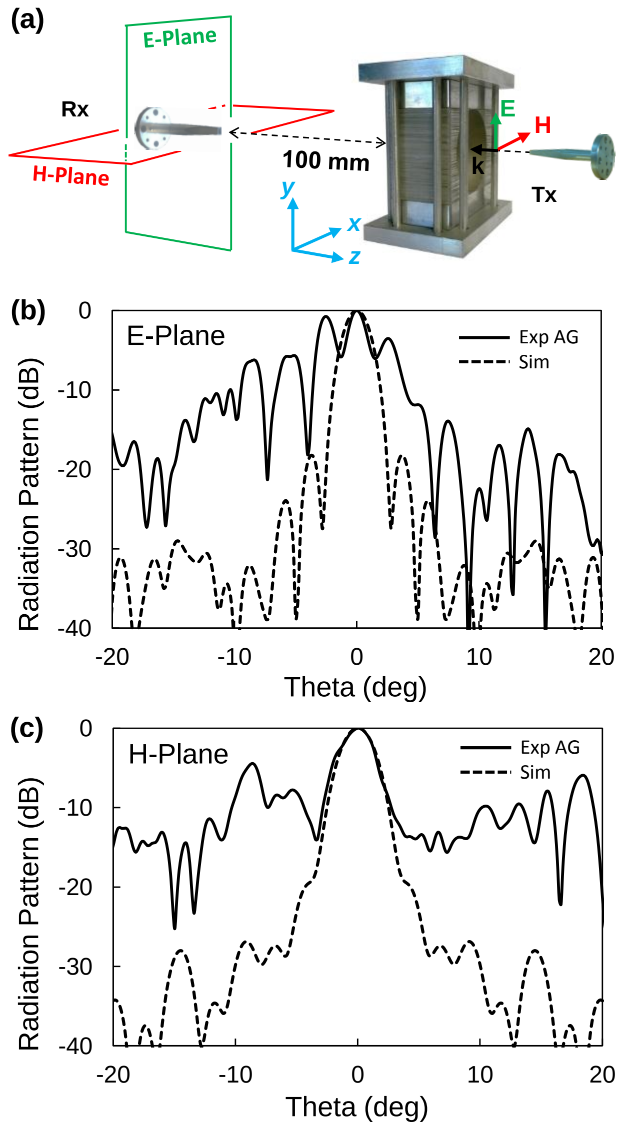

Fig. 5. (a) Sketch of the experimental set-up used for the far-field characterization. Measured and simulated co-polar radiation pattern on the E-plane (b) and H-plane (c).

On the E-plane (Fig. 5(b)) a very narrow main lobe is obtained experimentally, pointing exactly in the direction of the optical axis (0 deg), with a half-power beamwidth (HPBW) of 1.6 deg and FNBW equal to 2.8 deg. In the simulation a slightly wider main lobe is obtained with a HPBW and FNBW of 2.2 deg and 5.6 deg, respectively. It can be noticed that the experimental radiation pattern presents higher secondary lobes that we attribute to some undesired effect during measurement and the absence of the WR-5.1 probe in the modeling. In the simulation the first side-lobe level (FSLL) is -18.3 dB while in the experiment are of -3.6 dB and -0.8 dB at both sides of the main lobe. The cross-polar component, measured with the receiving antenna rotated 90 deg with respect to the incident vertical electric field, is rather low, 34 dB lower than the co-polar one on the optical axis. On the H-plane, presented in Fig. 5(c), the main lobe also points along the optical axis. In this plane, the beamwidth is wider, with a HPBW=3.0 deg, and also the angle between first nulls FNWB=8.2 deg which is in very good agreement with the simulated values. In this plane, the level of the secondary lobes is much lower: -13.8 dB and -7.8 dB. Finally, the measured directivity is equal to 17.6 dBi, somewhat away from the 25.4 dBi predicted by the ideal simulation. This difference arises manly from the penalty introduced by the high secondary lobes in the experimental E-plane. A comparison of all these results is presented in Table II.

TABLE II
RADIATION PATTERN PARAMETERS

	HPBW[a]		**FNBW**[b]		**FSLL**[c]		**Directivity**
	E-Plane	*H-Plane*	*E-Plane*	*H-Plane*	*E-Plane*	*H-Plane*	
Exp AG	1.6 deg	3.0 deg	2.3 deg	8.2 deg	-3.6 dB	-13.8 dB	17.6 dBi
Sim	2.2 deg	2.9 deg	5.6 deg	7.8 deg	-18.3 dB	-19.3 dB	25.4 dBi

[a]HPBW is the half-power beamwidth
[b]FNBW is the first null beam width
[c]FSLL is the first side-lobe level

IV. CONCLUSIONS

We present in this work the performance of a metallic ENZ lens with a plano-concave profile working at 144 GHz. The ENZ behavior is achieved by means of an array of narrow waveguides working very close to the cut-off frequency of the fundamental mode, being the first realization of this kind of ENZ medium in this frequency regime. The array of 33 × 111 hollow waveguides with height equal to $\lambda_0/42$ in a lens thickness between $6\lambda_0$ and $26\lambda_0$ has been assembled after a challenging fabrication process. The lens has been characterized systematically within a combined experimental and computational approach to study the impact of the tolerances and the invasiveness of the two different probes used experimentally. Experimental measurements at millimeter-waves show, for the two setups used, a clear focus in both E- and H-planes with a maximum transmission enhancement of 15.90 dB when the ENZ lens is uniformly illuminated, resulting in a good performance of the lens compared to previous metallic lenses. A directivity of 17.6 dBi is measured with very low values of cross-polar components on the E- and H-plane. The results underline that homogenization of the lens can be carried out, which has strong implications for fundamental physics and device engineers. This work opens new possibilities of using waveguide-based ENZ metamaterials on applications such as graded-index lenses, prisms or beam steerers at millimeter-wave.

ACKNOWLEDGMENT

The authors are in debt to the technology center Tekniker for the precise fabrication of the lens. The authors dedicate this work to the memory of their beloved colleague and friend, the late Prof. Mario Sorolla, who enthusiastically encouraged the fabrication and experimental characterization of the lens.

REFERENCES

[1] N. Engheta and Z. Ziolkowski, *Metamaterials: Physics and engineering exploration*, New York: Wiley, 2006.
[2] M. Silveirinha and N. Engheta, “Tunneling of electromagnetic energy through Subwavelength channels and bends using ε-near-zero materials,” *Phys. Rev. Lett.*, vol. 97, no. 15, pp. 1–4, Oct. 2006.
[3] J. D. Jackson, *Classical electrodynamics*, New York: Wiley, 1999.
[4] R. Maas, J. Parsons, N. Engheta, and A. Polman, “Experimental realization of an epsilon-near-zero metamaterial at visible wavelengths,” *Nat. Photonics*, vol. 7, no. 11, pp. 907–912, Oct. 2013.
[5] P. Moitra, Y. Yang, Z. Anderson, I. I. Kravchenko, D. P. Briggs, and J. Valentine, “Realization of an all-dielectric zero-index optical metamaterial,” *Nat. Photonics*, vol. 7, no. 10, pp. 791–795, Aug. 2013.
[6] M. Silveirinha and N. Engheta, “Theory of supercoupling, squeezing wave energy, and field confinement in narrow channels and tight bends using ε near-zero metamaterials,” *Phys. Rev. B*, vol. 76, no. 24, pp. 1–17, Dec. 2007.
[7] B. Edwards, A. Alù, M. Young, M. Silveirinha, and N. Engheta, “Experimental verification of epsilon-near-zero metamaterial coupling and energy squeezing using a microwave waveguide,” *Phys. Rev. Lett.*, vol. 100, no. 3, pp. 1–4, Jan. 2008.
[8] A. Alù, M. Silveirinha, A. Salandrino, and N. Engheta, “Epsilon-near-zero metamaterials and electromagnetic sources: Tailoring the radiation phase pattern,” *Phys. Rev. B*, vol. 75, no. 15, pp. 1–13, Apr. 2007.
[9] R. Ziolkowski, “Propagation in and scattering from a matched metamaterial having a zero index of refraction,” *Phys. Rev. E*, vol. 70, no. 4, pp. 1–12, Oct. 2004.
[10] B. Edwards, A. Alù, M. Silveirinha, and N. Engheta, “Experimental verification of plasmonic cloaking at microwave frequencies with metamaterials,” *Phys. Rev. Lett.*, vol. 103, no. 15, p. 153901, Oct. 2009.
[11] A. Monti, F. Bilotti, A. Toscano, and L. Vegni, “Possible implementation of epsilon-near-zero metamaterials working at optical frequencies,” *Opt. Commun.*, vol. 285, no. 16, pp. 3412–3418, Dec. 2012.
[12] M. G. Silveirinha, C. R. Medeiros, C. A. Fernandes, and J. R. Costa, “Resolving subwavelength objects with a crossed wire mesh superlens operated in backscattering mode,” *New J. Phys.*, vol. 13, no. 5, p. 053004, May 2011.
[13] C. Argyropoulos, P.-Y. Chen, G. D’Aguanno, N. Engheta, and A. Alù, “Boosting optical nonlinearities in ε-near-zero plasmonic channels,” *Phys. Rev. B*, vol. 85, no. 4, p. 045129, Jan. 2012.
[14] N. Engheta, “Circuits with light at nanoscales: optical nanocircuits inspired by metamaterials.,” *Science*, vol. 317, no. 5845, pp. 1698–702, Sep. 2007.

[15] Y. Sun, B. Edwards, A. Alù, and N. Engheta, "Experimental realization of optical lumped nanocircuits at infrared wavelengths.," *Nat. Mater.*, vol. 11, no. 3, pp. 208–12, Mar. 2012.
[16] W. Kock, "Metal-lens antennas," *Proceedings of the IRE*, vol. 34, no. 11, pp. 828–836, Nov. 1946.
[17] M. Navarro-Cía, M. Beruete, I. Campillo, and M. Sorolla, "Enhanced lens by ε and μ near-zero metamaterial boosted by extraordinary optical transmission," *Phys. Rev. B*, vol. 83, no. 11, pp. 1–5, Mar. 2011.
[18] V. Pacheco-Peña, B. Orazbayev, V. Torres, M. Beruete, and M. Navarro-Cía, "Ultra-compact planoconcave zoned metallic lens based on the fishnet metamaterial," *Appl. Phys. Lett.*, vol. 103, no. 18, p. 183507, Oct. 2013.
[19] R. Mendis and D. M. Mittleman, "A 2-D Artificial Dielectric With $0 \leq n < 1$ for the Terahertz Region," *IEEE Trans. Microw. Theory Tech.*, vol. 58, no. 7, pp. 1993–1998, Jul. 2010.
[20] J. Liu, R. Mendis, and D. M. Mittleman, "A Maxwell's fish eye lens for the terahertz region," *Appl. Phys. Lett.*, vol. 103, no. 3, p. 031104, Jul. 2013.
[21] M. Navarro-Cía, M. Beruete, M. Sorolla, and N. Engheta, "Lensing system and Fourier transformation using epsilon-near-zero metamaterials," *Phys. Rev. B*, vol. 86, no. 16, p. 165130, Oct. 2012.
[22] V. Torres, V. Pacheco-Peña, P. Rodríguez-Ulibarri, M. Navarro-Cía, M. Beruete, M. Sorolla, and N. Engheta, "Terahertz epsilon-near-zero graded-index lens.," *Opt. Express*, vol. 21, no. 7, pp. 9156–66, Apr. 2013.
[23] L. Verslegers, P. B. Catrysse, Z. Yu, J. S. White, E. S. Barnard, M. L. Brongersma, and S. Fan, "Planar lenses based on nanoscale slit arrays in a metallic film.," *Nano Lett.*, vol. 9, no. 1, pp. 235–8, Jan. 2009.
[24] S. Ishii, V. M. Shalaev, and A. V Kildishev, "Holey-metal lenses: sieving single modes with proper phases.," *Nano Lett.*, vol. 13, no. 1, pp. 159–63, Jan. 2013.
[25] T. W. Ebbesen, H. Lezec, H. Ghaemi, T. Thio, and P. Wolff, "Extraordinary optical transmission through sub-wavelength hole arrays," *Nature*, vol. 391, no. 6668, pp. 667–669, Feb. 1998.
[26] D. M. Pozar, *Microwave Engineering*, New York: Wiley, 2005.
[27] S. Gregson, J. McCormick, and C. Parini, *Principles of planar near-field antenna measurements*, London: Institute of Engineering and Technology, 2007.
[28] S. Lucyszyn, "Investigation of anomalous room temperature conduction losses in normal metals at terahertz frequencies," *IEE Proc. - Microwaves, Antennas Propag.*, vol. 151, no. 4, p. 321, Aug. 2004.

Víctor Torres was born in Pamplona, Spain, in 1985. He received the degree in Telecommunication Engineering and the M.Sci. degree in Communication Technologies from the Public University of Navarre, Navarre, Spain, in 2009, and 2010, respectively.

He is currently working as a Postdoctoral Researcher in the Millimeter and Terahertz Waves and Plasmonic Laboratory of the Electrical and Electronic Engineering Department, Public University of Navarre, Pamplona, Spain. His current research interests are mainly aimed on metamaterials, permittivity near zero structures, extraordinary transmission applications, plasmonics, nanoantennas, and millimeter, terahertz and infrared frequencies.

Bakhtiyar Orazbayev was born in Kazakhstan, in 1988. He received the degree in Physics from People's Friendship University of Russia (PFUR), Moscow, Russia, in 2011.

He is currently working as a Predoctoral Researcher in the Millimeter and Terahertz Waves and Plasmonic Laboratory of the Electrical and Electronic Engineering Department, Public University of Navarre, Pamplona, Spain. His current research interests are mainly aimed on metamaterials, permittivity near zero structures, extraordinary transmission applications.

Víctor Pacheco-Peña was born in San Salvador, El Salvador, in 1988. He received the degree in Telecommunication engineering from Universidad Don Bosco (UDB), Soyapango, El Salvador, in 2011. He received the M.Sc. degree in communication technologies from the Public University of Navarre, Navarre, Spain, in 2012.

He is currently working as a Predoctoral Researcher with the Millimeter and Terahertz Waves and Plasmonic Laboratory in the Electrical and Electronic Engineering Department, Public University of Navarre, Pamplona, Spain. His current research interests are mainly aimed on metamaterials, permittivity near zero structures, extraordinary transmission applications, lenses and millimeter and terahertz frequencies.

Jorge Teniente was born in Lodosa, Spain, in 1973. He received the M.Sc. and Ph.D. degrees in telecommunications engineering from the Public University of Navarra (UPNA), Pamplona, Spain, in 1997 and 2003, respectively.

Since 1997, he has been with the Antenna Group, Public University of Navarra, where he is currently an Associate Professor and has been involved in the research activity of his research group. Between 1999 and 2000, he was a Spanish Trainee with the ESA/ESTEC, Noordwijk, The Netherlands. In Summer 2002, he was a Research Scientist with the ESA project "StarTiger 1" at the Rutherford Appleton Laboratory, Didcot, U.K. From 2004 to 2005, he was with the University of Oviedo, Asturias, Spain. His current area of research is in the field of horn antenna technology with emphasis on corrugated horns and space and radio telescope antenna applications. Also, he is involved in terahertz technologies, subsystems, and devices.

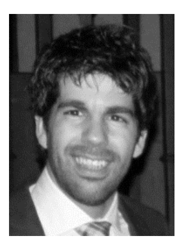

Miguel Beruete was born in Pamplona, Spain, in 1978. He received the M.Sci. and Ph.D. degrees in telecommunication engineering, from the Public University of Navarre (UPNA), Navarre, Spain, in 2002 and 2006, respectively.

From September 2002 to January 2007, he was working as Predoctoral Researcher (FPI fellowship recipient) in the Electrical and Electronic Engineering Department, Public University of Navarre. From January to March 2005 he worked as visiting researcher at the University of Seville, as a part of his doctoral research.

From February 2007 to September 2009 he was at the electronics department of the technological center CEMITEC in Noain (Navarre), developing, designing and measuring high frequency communication devices.

In September 2009 he joined the TERALAB at UPNA, as a post-doc Ramón y Cajal fellow researcher under the supervision of Prof. Mario Sorolla.

In March 2014, he joined the Antennas Group-TERALAB of UPNA, where he supervises several Ph.D. and M.Sci. Theses and is responsible of the TERALAB laboratory.

Dr. Beruete has authored more than 70 articles, one book chapter, 3 patents and more than 150 conference communications. He has been awarded with the PhD Prize of the Public University of Navarre (2006-2007) to the best Doctoral Thesis in the year 2006-2007, 2 CST University Publication Awards to the best international journal publication using CST in the years 2005 and 2012, and the XII Talgo Award of Technological Innovation in 2011. His research interests include metamaterials, plasmonics, extraordinary transmission structures, leaky-wave antennas, nanoantennas, and in general quasioptical devices from microwaves to infrared frequencies, with special interest in the terahertz range.

Miguel Navarro-Cía (S'08–M'10) was born in Pamplona, Spain, in 1982. He received the M.Sci. and Ph.D. degrees in Telecommunication Engineering, and M.Res. degree in Introduction to Research in Communications from the Public University of Navarre, Navarre, Spain, in 2006, 2010 and 2007, respectively.

From September 2006 to January 2010, and from February 2010 until March 2011, he was working as Predoctoral Researcher (FPI fellowship recipient) and Research Associate in the Electrical and Electronic Engineering Department, Public University of Navarre, respectively. From March 2011 until March 2012, and from then until December 2012, he was Research Associate at Imperial College London and University College London, respectively. Currently he is Junior Research Fellow in the Optical and Semiconductor Devices Group, Imperial College London. He is also affiliated with the Centre for Terahertz Science and Engineering, and the Centre for Plasmonics and Metamaterials at Imperial College London, and as a Visiting Researcher with the University College London. Also, he worked as Visiting Researcher at University of Pennsylvania for 3 months in 2010, at Imperial College London in 2008, 2009 and 2010 for 4, 6 and 3 months, respectively, and at Valencia Nanophotonics Technology Center for 2 months in 2008. His current research interests are focused on plasmonics, near-field time-domain spectroscopy, metamaterials, antennas, complex surface waves, frequency selective surfaces, and millimeter, terahertz and infrared frequencies.

Dr. Navarro-Cía is member of the Optical Society of America, the European Association on Antennas and Propagation (EurAAP), and the Spanish National Association and Professional Board of Telecommunication Engineers. He was awarded with the Best Doctoral Thesis in Basic Principles and Technologies of Information and Communications, and Applications corresponding to the XXXI Edition of Awards "Telecommunication Engineers" 2010 and is recipient of the 2011 Junior Research Raj Mittra Travel Grant.

Mario Sorolla Ayza (S'82–M'83–SM'01) was born in Vinaròs, Spain, in 1958. He received the Telecommunication Engineer degree from the Politechnical University of Catalonia, Barcelona, Spain, in 1984 and the Ph.D. degree from the Politechnical University of Madrid, Madrid, Spain, in 1991.

From 1986 to 1990, he designed very high power millimeter waveguides for plasma heating in the Euratom-Ciemat Spanish Nuclear Fusion Experiment and was an Invited Scientist at the Institute of Plasma Research at Stuttgart University, in Germany, from 1987 to 1988. He worked in microwave integrated circuits and monolithic microwave integrated circuits for satellite communications for industries. From 1984 to 1986, he was a Professor at the Politechnical University of Catalonia, and from 1991 to 1993, at Ramon Llull University in Barcelona. Since 1993, he has been a Professor at the Public University of Navarre, Navarre, Spain. His interest range from high-power millimeter waveguide components and antennas, coupled wave theory, quasioptical systems in the millimeter wave and terahertz range and applications of metamaterials and enhanced transmission phenomena to microwave circuits and antennas.

Dr Sorolla Ayza passed away on November 1, 2012.

Nader Engheta (S'80–M'82–SM'89–F'96) received the B.S. degree in electrical engineering from the University of Tehran, Tehran, Iran, and the M.S. and Ph.D. degrees in electrical engineering from the California Institute of Technology (Caltech), Pasadena.

He is the H. Nedwill Ramsey Professor at the University of Pennsylvania, with affiliation in the departments of Electrical and Systems Engineering, Bioengineering, Materials Science and Engineering, and Physics and Astronomy. After spending one year as a postdoctoral research fellow at Caltech and four years as a Senior Research Scientist at Kaman Sciences Corporation's Dikewood Division, he joined the faculty of the University of Pennsylvania. He is also a member of the Mahoney Institute of Neurological Sciences. He was the graduate group chair of electrical engineering from 1993 to 1997. Selected as one of the Scientific American Magazine 50 Leaders in Science and Technology in 2006 for developing the concept of optical lumped nanocircuits, he is a Guggenheim Fellow, an IEEE Third Millennium Medalist, a Fellow of the American Physical Society (APS), Optical Society of America (OSA), American Association for the Advancement of Science (AAAS), and of the SPIE-International Society for Optical Engineering. He is the recipient of the 2014 Balthasar van der Pol Gold medal from URSI (International Union of Radio Science), the 2013 Inaugural SINA award in engineering, 2013 Benjamin Franklin Key award, the 2012 IEEE

Electromagnetics Award, the 2008 George H. Heilmeier Award for Excellence in Research, the Fulbright Naples Chair Award, NSF Presidential Young Investigator award, UPS Foundation Distinguished Educator term Chair, and several teaching awards. He was an Associate Editor of the IEEE ANTENNAS AND WIRELESS PROPAGATION LETTERS (2002–2007), of the IEEE TRANSACTIONS ON ANTENNA AND PROPAGATION (1996–2001), and *Radio Science* (1991–1996). He was on the Editorial Board of the *Journal of Electromagnetic Waves and Applications,* and of *Metamaterials*. He is currently on the Editorial board of *Physical Review X* (PRX) of the American Physical Society, of *Waves in Random and Complex Media*, of *Nanophotonics*, and of the *Istituto Superiore Mario Boella Book Series in Radio Science*. He served as an IEEE Antennas and Propagation Society Distinguished Lecturer for the period 1997–1999. He is a member of Sigma Xi, Commissions B, D, and K of the U.S. National Committee (USNC) of the International Union of Radio Science (URSI), and a member of the Electromagnetics Academy. He was the Chair of the Commission B of USNC-URSI for 2009–2011 and of the Gordon Research Conference on Plasmonics in 2012. His current research interests and activities span over a broad range of areas including metamaterials and plasmonics, nanooptics and nanophotonics, nanocircuits and nanostructures modeling, graphene photonics, one-way flow of photons, bio-inspired/biomimetic polarization imaging and reverse engineering of polarization vision, miniaturized antennas and nanoantennas, hyperspectral sensing, biologically-based visualization and physics of sensing and display of polarization imagery, fields and waves phenomena, fractional operators and fractional paradigm in electrodynamics. He has guest edited/co-edited several special issues, including the special issue of the *Journal of Electromagnetic Waves and Applications* on "Wave Interaction with Chiral and ComplexMedia" in 1992, part special issue of the *Journal of the Franklin Institute* on "Antennas and Microwaves" in 1995, special issue of *Wave Motion* on "Electrodynamics in Complex Environments" in 2001, special issue of the IEEE TRANSACTIONS ON ANTENNAS AND PROPAGATION on "Metamaterials" in 2003, special issue of *Solid State Communications* on "Negative Refraction and Metamaterials for Optical Science and Engineering" in 2008, special issue of the IEEE JOURNAL OF SELECTED TOPICS IN QUANTUM ELECTRONICS on "Metamaterials" in 2010, the special issue of the *Proceedings of IEEE* on "Metamaterials: Fundamentals and Applications in Microwaves and Optical Regimes" in 2011, and the special section of the *Physical Review X* (PRX) on metamaterials. He co-edited the book "*Metamaterials: Physics and Engineering Explorations*" by Wiley—IEEE Press, 2006.